

Numerical Simulation Analyses of Single Lap Joints for Wood-PE Composites Formed with Epoxy and Acrylic Ester Adhesives

Dongyan Zhou and Mingwei Di *

Wood powder/polyethylene composites (WP/PE) were surface treated by plasma discharge and bonded with epoxy resin and acrylic ester adhesives, respectively. The finite element model of the single lap bonded joints of WP/PE was established through the elastic-plastic finite element method, and the influences of adhesive and lap length on the stress distribution in the adhesive joints were analyzed. The results showed that polar oxygen-containing groups were introduced to the WP/PE surface with the plasma treatment, which improved the bonding properties. The peak values of Mises equivalent stress, peel stress, and shear stress of the bonded joints were mainly concentrated at the end of the bond joint. The peak values of the stress in the lap zone of the high-modulus epoxy resin-bonded joints were higher than those of the low-modulus acrylic ester-bonded joints. With an increased length of the joints, the Mises equivalent stress peak value at the end increased slightly, the peeling stress peak value decreased slightly, and the shear stress peak value changed little. The elastic modulus of the adhesive had a great influence on the stress distribution, and the change in the lap length was not remarkable enough to improve the stress distribution of the adhesive joint.

Keywords: Wood powder/polyethylene composites; Single lap bonded joints; Stress distribution; Finite element numerical analysis; Elastic modulus of adhesive

Contact information: Key Laboratory of Bio-Based Material Science & Technology (Ministry of Education), Northeast Forestry University, Harbin, China; *Corresponding author: dimingwei@126.com

INTRODUCTION

Wood powder/polyethylene composites (WP/PE) are a new kind of composite material. It has been widely used in various fields because of its properties that come from combining both wood and plastic. This type of composite is mainly used in the field of building materials that require only moderate structural performance (Ashori 2008; Perisić *et al.* 2009), such as doors, windows, outdoor floors, railings, decorative panels, and vestibule boards. Also, WP/PE is widely used in urban public facilities, including newsstands, trash cans, and outdoor fitness equipment. It has great potential for use in transportation industries, such as in containers, aircraft seats, luggage compartments, and car seats. However, the extrusion forming method of WP/PE requires the fabrication of large-scale and complex-shaped products to be completed with the help of connection technology. Compared with welding and mechanical connections, adhesive bonding is a non-destructive seamless connection technology, which meets the requirements of a lightweight structural process design, simple operation, and short cycle (Hung *et al.* 2017). Seamless connections of WP/PE can be realized through adhesive bonding, which can make the connection part more beautiful, improve the appreciation of the product, and

realize the structural connection of complex forms (Ozdemir and Mengeloglu 2008; Cheng *et al.* 2012 a,b).

The low surface energy in non-polar nature of PE can lead to difficulties in bonding within a WP/PE composite (Gupta *et al.* 2007; Gupta and Laborie 2007; Oporto *et al.* 2007; Moritzer and Hopp 2017). Bonding can be realized only by surface treatment in advance. Different surface treatment methods (Liu *et al.* 2010) and different adhesives, which require a corresponding surface treatment, are needed to obtain the desired bonded joint for different bonding structures and applications in various environments. Plasma jet surface treatment is usually used because of its simple treatment process. The surface energy of treated WP/PE increases with the introduction of active oxygen groups, and the surface roughness of treated WP/PE increases because of the scouring jet atmosphere, which can greatly improve the bonding strength (Hünnekens *et al.* 2018; Yáñez-Pacios and Martín-Martínez 2018). Epoxy and acrylic ester adhesives are usually used for the bonding of surface-treated WP/PE composites (Dimitriou *et al.* 2016). Epoxy resin adhesive has a high elastic modulus, strong resistance to deformation, and complex curing process. In contrast, acrylic ester adhesive has a low elastic modulus and weak resistance to deformation, but its curing process is simple.

In the design of bonding structures (Wong and Liu 2017), stress concentration is easy to form at the connection part of a joint under external force, which eventually leads to joint failure. Adhesive plays a role in transferring the load on the joint, so adhesive selection is important to bonded joints. The mechanical properties of bonded joints, such as the strength and failure, can be determined by an experimental method (You *et al.* 2003; da Silva *et al.* 2010; Ayatollahi *et al.* 2017; Soroceanu *et al.* 2017), but it cannot describe the microstructure stress distribution of bonded joints. The stress distribution in bonded joints can be described by finite element analysis, which provides a technical scheme for the mechanical analysis of complex bonded structures (Özer and Öz 2012). Santoni conducted finite element simulation on the stiffness characteristics of wood-plastic composite materials to optimize the structural section and improve the acoustic performance of the structure (Santoni *et al.* 2018). The finite element method is used to analyze the failure process of bonded joints of wood-plastic composite materials, which is helpful to restrain the debonding of bonded layer (Tang and Liu 2018).

In this study, epoxy resin and acrylic ester adhesives were used to bond WP/PE after a jet plasma surface treatment. The mechanical properties of single lap wood-plastic joints with different adhesives and lap lengths under shear stress were analyzed. The stress distribution of the adhesive joints was analyzed to provide a theoretical basis and design ideas for selection of the complex adhesive parameters (Sen and Köksal 2015; Ribeiro *et al.* 2016).

EXPERIMENTAL

Materials

The WP/PE was self-made through extrusion molding. The raw material for the wood powder was poplar powder (Zhejiang Province, Deqing County-licensing, Lin Wood Flour Co. Ltd., China) that was 380 μm to 830 μm in size, and its mass fraction was 60%. The mass fraction of the high-density PE was 35 wt%, and the rest was 3 wt% compatibilizer maleic anhydride PE grafted and 2 wt% lubricant. The extruded WP/PE was cut into samples with a cutting machine. The shape of the samples was rectangular, and the

sizes of the samples were 40 mm × 25 mm × 4 mm. Epoxy resin (Heilongjiang Institute of Petrochemistry, Harbin, China) and two-component acrylic ester adhesives (Heilongjiang Institute of Petrochemistry, Harbin, China) were used for bonding. The epoxy resin adhesive (epoxy resin E-51 mixed with industrial polyamide curing agent with a mass ratio 1 to 1) was cured at room temperature for 24 h and then at 50 °C for 4 h. The acrylic ester adhesive was cured at room temperature for 24 h.

Surface Treatment

A GSL-1100X-PJF-A jet plasma processor (Shenyang Kejing Automation Equipment Co. Ltd., Shenyang, China) was used to treat the surface of the WP/PE. Plasma surface treatment was carried out at room temperature. The specimens were positioned vertically under the plasma beam in the device. The plasma jet atmosphere was air, and the discharge gap between the specimens and the plasma beam current was 30 mm, and the specimens were treated for 30 s, which produced the best bonding adhesion strength. Due to the ageing of plasma treated surface, the bonding of WP/PE with epoxy resin adhesive and acrylic ester adhesive respectively was completed within 1 h after the plasma treatment.

Tests and Analyses

The shear failure test of the adhesive joint was performed with the universal testing machine SANS-CMT5504 (XinSanSi Co. Ltd., Shenzhen, China) with a loading speed of 5 mm/min, according to ASTM D905-08 (2013). The FTIR spectral analysis with an ATR mode was conducted on a Magna-IR 560 Fourier transform infrared spectroscope provided by Nicolet Co. Ltd. (Madison, USA), with a resolution of 4 cm⁻¹ and a scanning range of 4000 cm⁻¹ to 400 cm⁻¹ to measure the functional groups on the surfaces of the untreated and surface-treated specimens. The bonded joint was simulated by the finite element method with the software Abaqus 6.13 (SIMULIA, Rhode Island, USA). The type and size of the joint are shown in Fig. 1.

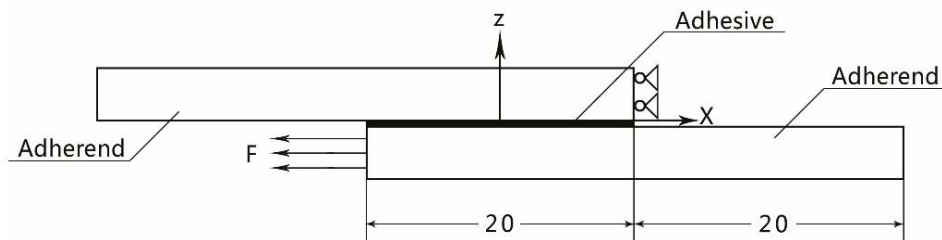


Fig. 1. Schematic diagram of the geometric size and loading constraint of the adhesive joints

RESULTS AND DISCUSSION

Bonding Strength

Figure 2 shows the compression shear strength of the untreated and plasma discharge-treated WP/PE adhesive joints bonded with the epoxy resin and acrylic ester adhesives. The figure shows that the untreated WP/PE bonded joint had an extremely low shear strength because of the non-polar PE composition on the material surface. Also, the adhesive strength of the joints bonded with the epoxy resin and acrylic ester adhesives was improved after the plasma treatment. It was observed that the plasma discharge process changed the surface properties of the WP/PE and improved the bonding force between the

material surface and adhesive (Noeske *et al.* 2004; Wolkenhauer *et al.* 2008). Thus, the bonding strength was greatly improved.

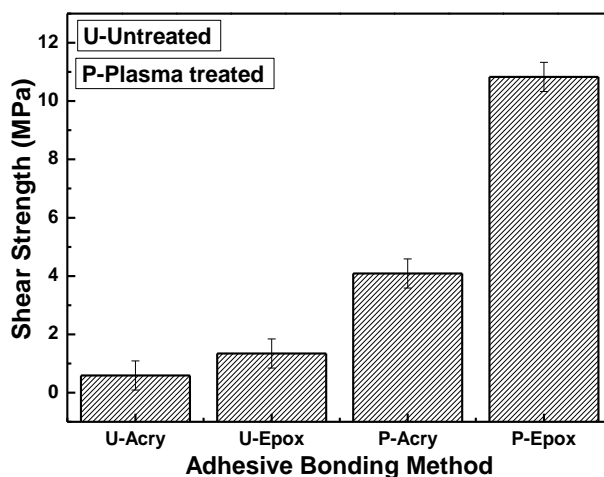


Fig. 2. Compression shear strength of the untreated and plasma-treated WP/PE adhesive joints

FTIR Analysis

Figure 3 shows the FTIR spectra of the untreated and plasma-treated WP/PE sample surfaces. The spectrum of the untreated sample showed -CH_2 symmetric stretching vibration (2914 cm^{-1}), antisymmetric stretching vibration (2848 cm^{-1}), in-plane bending vibration (1471 cm^{-1}), and C-H external bending vibration of the olefins (717 cm^{-1}). Also, it was indicated that the WP/PE surface was almost completely composed of PE, which is difficult to bond.

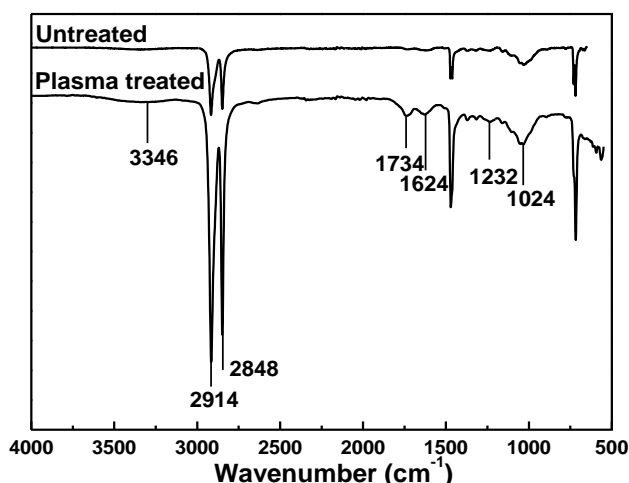


Fig. 3. FTIR spectra of the WP/PE surface before and after plasma treatment

Compared with the untreated sample, the spectrum of the plasma-treated sample showed stretching vibration absorption of C=O (1734 cm^{-1} and 1624 cm^{-1}), stretching vibration absorption of -OH (3346 cm^{-1}), and stretching vibration absorption of C-O (1024 cm^{-1} and 1232 cm^{-1}). This was because a large number of oxygen-containing groups, such as -COOH , -OH , and C-O, were introduced to the material surface by plasma discharge.

The introduction of these oxygen-containing groups changed the surface properties of the material and enhanced the bonding force between the adhesive molecules and surface of the treated WP/PE, which improved the bonding strength of the adhesive joint.

Failure Modes of the Adhesive Joints

Figure 4 shows the failure profile of the untreated and plasma-treated adhesive joints under compression shear stress. The quality of the adhesive joint can be tested by the strength of the adhesive joint, which is a direct evaluation, whereas the failure profile of the adhesive joint after the strength test is an indirect means to judge the quality of the adhesive joint. Figure 4 shows that the interface bonding strength of the untreated adhesive joint was low and the failure form of the adhesive joint was interfacial failure. The failure form of the adhesive joint after plasma treatment was mixed failure forms of cohesive failure and material body failure. The bonding strength of the adhesive joint was remarkably enhanced after the plasma treatment, and the results were consistent with the adhesive strength test. Moreover, Fig. 4 shows that the plasma-treated adhesive joints were all damaged, with the failure forms of material body failure at the edge of the overlap region, while there was partial interface damage inside of the overlap region. The reason for this phenomenon was not only that the adhesive joint may have had uneven internal defects, but also that the stress concentration of the adhesive joint was mainly distributed at the end of the overlap region, where the end of the overlap region was the starting point of fracture failure.

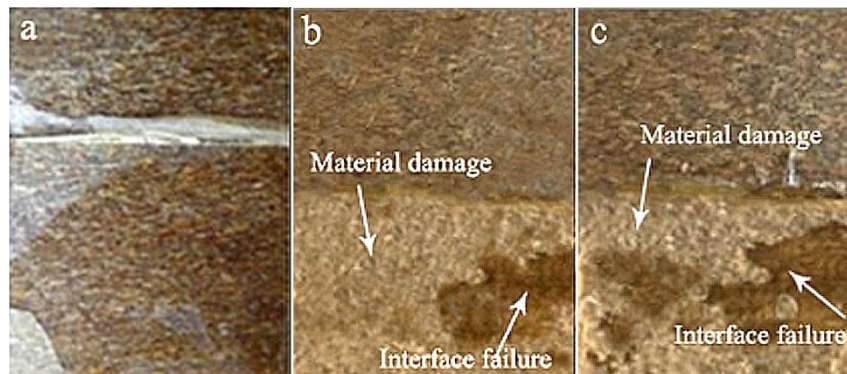


Fig. 4. Failure photos of the WP/PE bonded joints: (a) untreated epoxy resin adhesive; (b) plasma-treated epoxy resin adhesive; and (c) plasma-treated acrylic ester adhesive

Construction of the Finite Element Model

Taking the single lap bonded joint as an example, a simulation model was established using the Abaqus 6.13 finite element software. The distribution rules of the Mises equivalent stress, peeling stress, and shear stress in the elastic stage for the epoxy resin-bonded joints, acrylic ester-bonded joints, and the bonded joints with different lap lengths bonded with the above adhesives were analyzed by the elastic-plastic finite element method (Xará and Campilho 2018). The element was a hexahedral solid element, and the finite element mesh was a three-dimensional eight-node brick element. The overlapping area and adhesive layer were divided by a quadrilateral mesh with a 0.05-mm mesh size. When the lap length was changed, the mesh size of the lap area did not change. One end of the model was fixed, and the other side was loaded with an axial compressive shear load. To simulate the actual situation of the adhesive layer, a solid adhesive layer was added in

the middle of the overlap plate. The material parameters for the Abaqus CAE material setting module are given in Table 1, and the load (F) was 1 kN.

The Young's modulus (tensile modulus) and shear modulus of the material in table 1 were tested by universal mechanical testing machine in accordance with ASTM D638-14 (2015). The Poisson ratio of materials is calculated according to Eq. 1 (Huang *et al.* 2012).

$$G = \frac{E}{2(1+\nu)} \quad (1)$$

Table 1. Main Properties of the Materials and Adhesives in the Manuscript

Material	Young's Modulus (E) (GPa)	Poisson Ratio (ν)	Density (g/cm ³)
WP/PE Composite	2.200	0.30	1.1
Epoxy Resin Adhesive	1.900	0.38	1.02
Acrylic Ester Adhesive	0.230	0.35	0.965

To simplify the model analysis, the adhesive layer and bonded specimen were defined as isotropic elastoplastic materials by using the finite element numerical simulation models of (Sayman *et al.* 2013) and (Vaidya *et al.* 2008). It was assumed that the bonding structure was well connected, the bonded surface had no defects, the coupling joints had the same displacement, the joints were isotropic, and the bonding degree of the adhesive interface was 100%. Additionally, it was assumed that the bonded joint was in a small deformation state. The material nonlinearity was considered, while geometric nonlinearity was not considered.

Analysis of the Mises Equivalent Stress

Figure 5 shows the chart of the Mises equivalent stress for the WP/PE single lap joints bonded with epoxy resin and acrylic ester adhesives. The lap length was 20 mm. Equivalent stress is one of the mechanical parameters used to study the plastic deformation and fracture mechanism of metal materials.

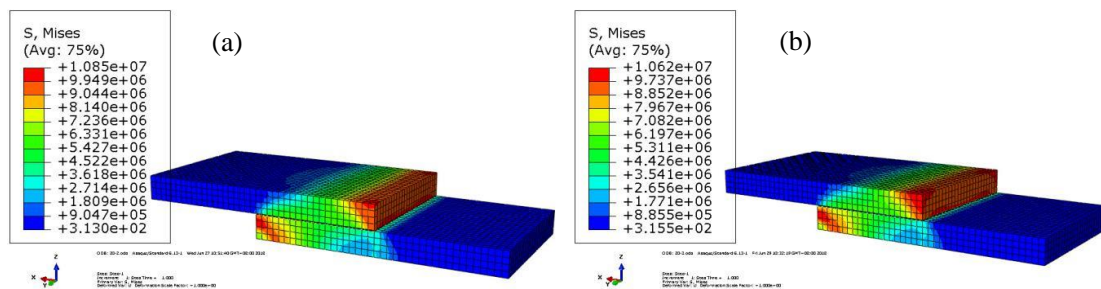


Fig. 5. Equivalent stress charts of the joints with (a) epoxy adhesive and (b) acrylic ester adhesive

At present, equivalent stress is widely used in the field of isotropic polymer materials with a good ductility. The change in the whole model was analyzed according to the stress distribution inside of the joint, and then the most dangerous area in the adhesive joint model was determined. Based on the fourth strength theory (Li 2012), the Mises equivalent stress

take into consideration that the specific energy of the shape change is the main cause of material failure. When elastic deformation occurred in the bonded structure under the action of an external force, the external force acted on the corresponding displacement part, which accumulated the deformation energy in the body. The failure point of the stress concentration was the reflection of the deformation energy in the bonded structure.

Figure 5 shows that the peak value of the Mises equivalent stress of the adhesive joints bonded with high- or low-modulus adhesives was distributed at the end of the lap zone, which indicated that the end of the lap zone was under a large load. This position was the most dangerous zone in the adhesive structure, and fracture failure of the joint usually began at the edge of the lap zone. The load of sticky material extended along the adhesive layer to the middle part of the joint, and the stress distribution was uniform. Also, the Mises stress peak of the high-modulus epoxy resin-bonded joint was 10.8 MPa, which was slightly larger than that of the low-modulus acrylic ester-bonded joint (10.6 MPa). When the elastic deformation of the epoxy resin-bonded joint structure occurred under load, the high modulus adhesive had a stronger ability to resist deformation. The energy accumulated in the process of resisting deformation for the bonded joint was larger, which resulted in a high stress peak. While the low-modulus acrylic ester adhesive had a poor ability to resist deformation and less energy was accumulated in the interior, the result was a relatively lower stress.

Figure 6 shows the Mises equivalent stress chart of the WP/PE single lap joints bonded with the epoxy resin and acrylic ester adhesives.

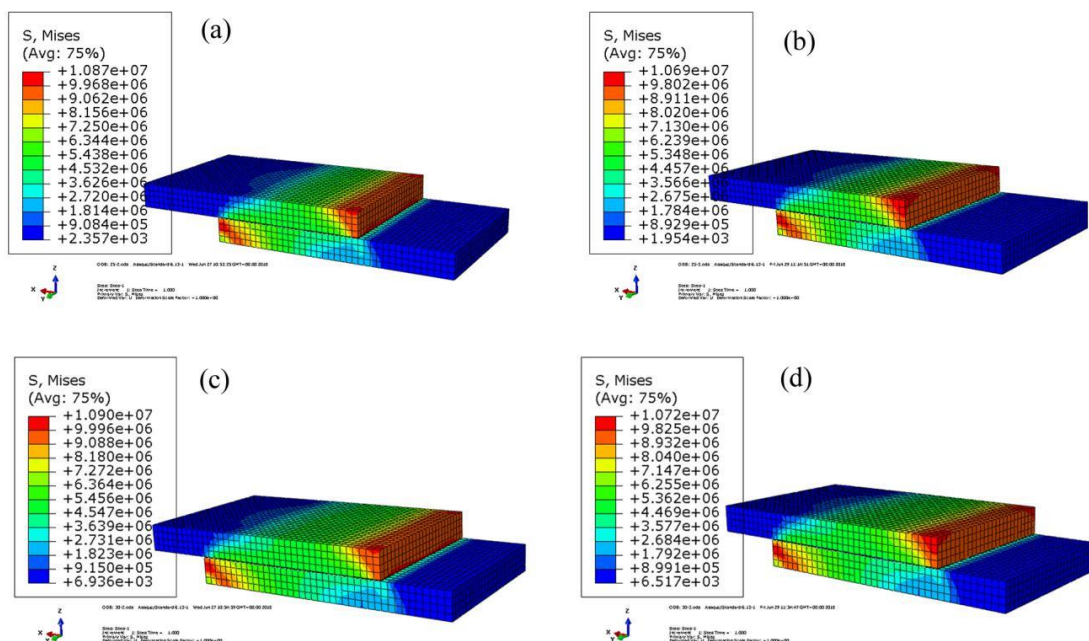


Fig. 6. Equivalent stress cloud diagrams of the adhesive joints with different lap lengths: (a) epoxy resin with a lap length of 25 mm; (b) acrylic ester with a lap length of 25 mm; (c) epoxy resin with a lap length of 30 mm; and (d) acrylic ester with a lap length of 30 mm

Figure 6 shows that the peak stress of the joints was distributed at the end of the lap zone, and the peak stress increased slightly with an increase in the lap length. This indicated that the stress concentration at the end of the glued joint had not been effectively improved

by increasing the lap length. The stress concentration near the end of the lap zone was the main reason for premature failure of the joint, which indicated that the potential of the adhesive had not been fully utilized, and the joint strength and efficiency had been reduced (Goglio *et al.* 2008; Shahin and Taheri 2009; Panigrahi 2013).

In summary, for the single lap bonded joints, the bending moment at the end of the bonded joints was caused by the non-coincidence of the loading line and the geometric center line, which led to uneven stress distribution on the specimen. The stress value at the end of the joint was the largest, which was the dangerous point in the joint, as is shown in Fig. 7.

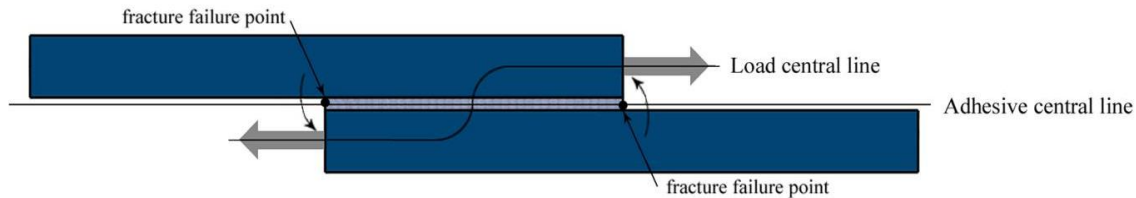


Fig. 7. Schematic diagram of the bending moment of the single lap adhesive joints

Analysis of the Stripping Stress

Figure 8 shows the axial peeling stress chart of single lap joints bonded with epoxy resin and acrylic ester adhesives along the Z-axis. The Z-axis peeling stress of the bonded structure was the stress distribution along the thickness direction of the bonded structure, which was caused by the bending moment resulting from the load deviating from the axis of the single lap specimen (Fig. 7). The direction of peeling stress was perpendicular to the bonded surface. The peel stress chart in Fig. 8 shows that the stress at the end of the overlap zone of the two adhesives was the greatest, which was not beneficial to the load bearing capacity of the adhesive layer. Also, Fig. 8 shows that the end of the overlap zone on the upper surface of the bonded structure took tensile stress and showed positive stress. As a result, the upper and lower surfaces of the overlap zone of the bonded joint had a good interfacial bond, the end of the overlap zone on the lower surface of the bonded joint showed negative compressive stress along the Z-axis, and the compressive stress on the lower surface hindered the destructive effect of the tensile stress on the upper surface of the joint. This showed that the peeling stress changing from positive tensile stress to negative compressive stress was helpful for improving the bearing capacity of the bonded joint.

Figure 8 shows that the peeling stress peak values of the high-modulus epoxy resin-bonded joint and low-modulus acrylic ester-bonded joint were 6.28 MPa and 4.91 MPa, respectively. Thus, the peeling stress of the high-modulus epoxy resin-bonded joint could be obtained, and it was larger than that of the low-modulus acrylic ester-bonded joint. This was mainly related to the small stiffness of the low-modulus acrylic ester adhesive, which increased the deformation of the bonded joints after loading. The small bending moment resulting from load deviation led to a uniform stress distribution (Mekaouche *et al.* 2015). When the stiffness of the adhesive under load was lower, the deformation was greater, so that the stress of the low-modulus adhesive joint was released, which resulted in the lower stress value of the joint. Therefore, the low-elastic modulus acrylic ester adhesive was suitable for engineering structures with small size changes. It should be noted that the increase in the deformation of the adhesive joint would cause the adhesive layer to crack

easily and the strength to fail, which was also the main reason for the low adhesive strength of the acrylic ester adhesive joint.

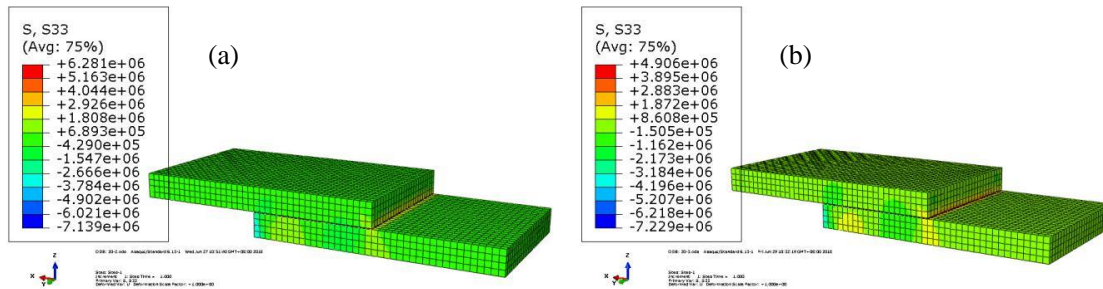


Fig. 8. Diagrams of the peeling stress of the joints with (a) epoxy adhesive and (b) acrylic ester adhesive

Figure 9 shows the peeling stress of the WP/PE single lap bonded joints with different lap lengths bonded by the epoxy resin and acrylic ester adhesives. It is shown that the peeling stress of the bonded joints was mainly distributed at the end of the lap zone. The peeling stress decreased slightly with an increase in the lap length, which indicated that the increase in the lap length was beneficial to the reduction of the peeling stress of the joint, but the effect was weak.

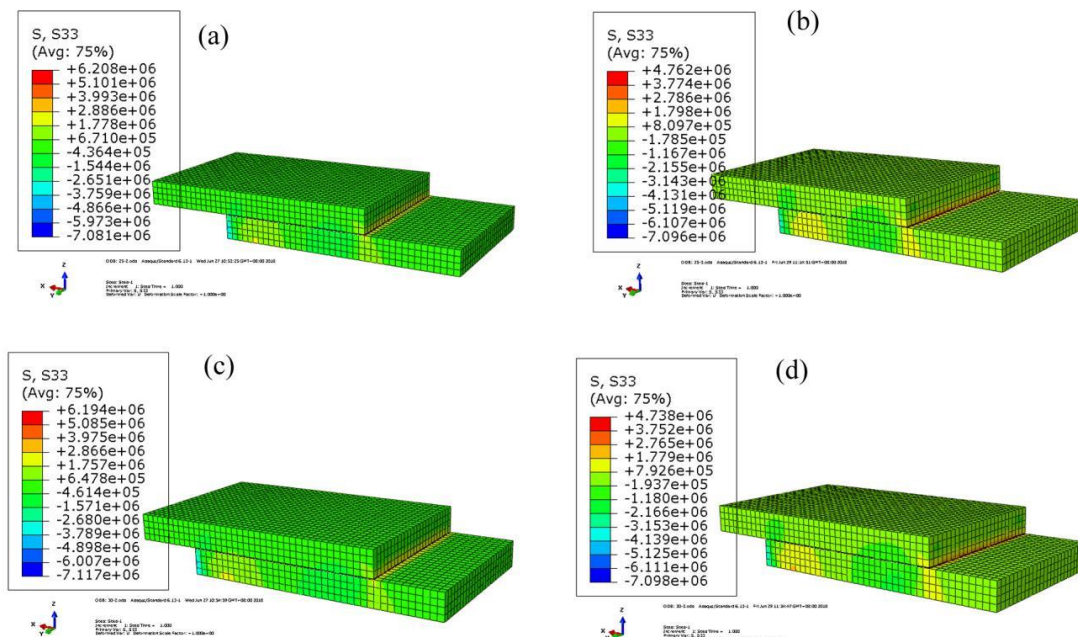


Fig. 9. Peel stress charts of the adhesive joints with different lap lengths: (a) epoxy resin with a lap length of 25 mm; (b) acrylic ester with a lap length of 25 mm; (c) epoxy resin with a lap length of 30 mm; and (d) acrylic ester with a lap length of 30 mm

It should be noted that the increase in the lap length would have resulted in the increase of internal defects in the adhesive layer, thereby reducing the bearing capacity of the adhesive joint. Therefore, in the design of the bonding structure, when the overlap

length was longer, the strength and stress distribution of the structure were better. In conclusion, the peeling stress of the single lap adhesive joint mainly depended on the elastic modulus of the adhesive, and the lap length had little effect on the peeling stress.

Analysis of the Shear Stress

Figure 10 shows the shear stress distribution of the single lap joints bonded with epoxy resin and acrylic ester adhesives. Figure 10 shows that the peak shear stress was distributed at the end of the bonded joint, and the load was transmitted mainly by two extremely narrow areas at the edge of the overlap zone (Nemeş and Lachaud 2010; Süliü 2018), which was unfavorable to the bearing capacity of the joint. The shear stress chart also showed that the shear stress peak value at the end of the high-modulus epoxy resin-bonded joint was 5.70 MPa, which was larger than that at the end of the low-modulus acrylic ester-bonded joint (4.42 MPa). The large deformation at the end of the low-modulus acrylic ester adhesive joint resulted in the release of stress in the overlap zone and the low peak stress at the end of the joint.

The peak stress at the end of the epoxy resin-bonded joint was higher, which indicated that the load-carrying capacity of the lap zone decreased within a unit length. Considering that the high-modulus epoxy resin adhesive had a higher bonded strength and the increase range of the load-bearing capacity of the bonded joint was greater than that of the load-bearing capacity decrease caused by stress concentration, when designing bonding structures, epoxy resin adhesives should be used for bonding structures with a higher bonding strength, while acrylic ester adhesives should be used for bonding structural parts with lower bonding strength requirements in the non-load-bearing overlap zone and smaller position changes.

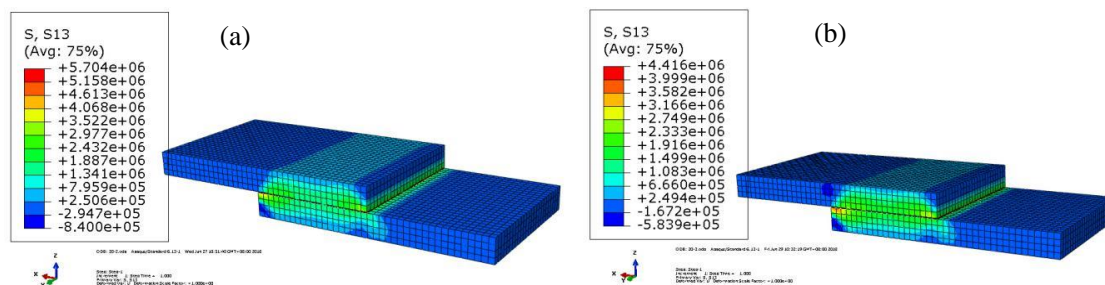


Fig. 10. Shear stress charts of the joints with (a) epoxy adhesive and (b) acrylic ester adhesive

Figure 11 shows the shear stress of the WP/PE single lap joint bonded with epoxy resin and acrylic ester adhesives. Figure 11 shows that the shear stress distributions of the adhesive bonded joints were basically the same, the peak shear stress distributions were at the end of the lap zone, and the peak shear stress values changed little with an increase in the lap length. The peak stress values at the end of the epoxy resin-bonded joints were higher than those of the acrylic ester bonded joints under the two lap lengths.

The above analysis showed that the improvement in the shear stress concentration at the end of the adhesive bonded joints by increasing the lap length was limited, and the effect of increasing the bearing capacity of the bonded joints by increasing the lap length was not obvious. Therefore, it was concluded that the shear stress of the single lap adhesive joint depended on the elastic modulus of the adhesive, and the effect of the lap length on the shear stress of the single lap adhesive joint was weak.

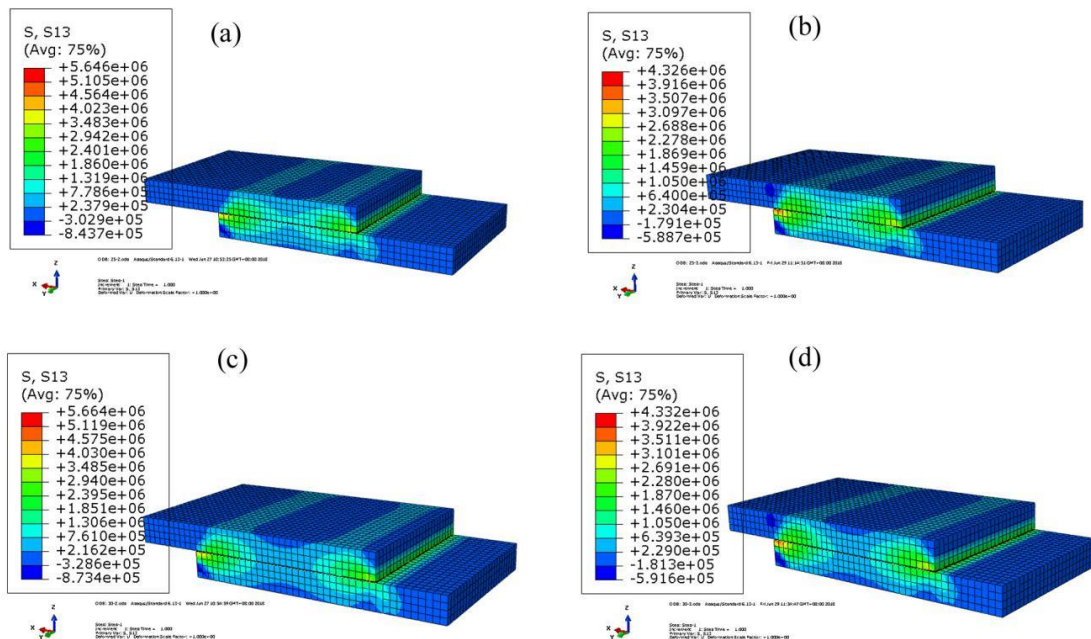


Fig. 11. Shear stress cloud charts of the adhesive joints with different lap lengths: (a) epoxy resin with a lap length of 25 mm; (b) acrylic ester with a lap length of 25 mm; (c) epoxy resin with a lap length of 30 mm; and (d) acrylic ester with a lap length of 30 mm

The failure mechanism of bonded joints could also be analyzed using the finite element simulation results. For the WP/PE bonded joints, the peak values of the equivalent stress, peeling stress, and shear stress at the end of the lap zone were the largest. Thus, under the action of external stress, the initial crack would appear at the end of the lap zone first and then follow the direction of the adhesive layer. During crack propagation, cohesive failure and interface failure would occur in the adhesive layer. The volume shrinkage of the adhesive during the curing process would cause certain shrinkage stress, and the existence of internal stress would aggravate the formation of micro-cracks in the joint (Zhang *et al.* 2018). The volume shrinkage rate of the epoxy resin adhesive was small, its internal stress was small, and the destructive force of the micro-cracks was also relatively small. However, because of the presence of double bonds, the volume shrinkage and internal stress of the acrylic ester adhesive after curing was larger, which aggravated the micro-cracks in the bonding area to the middle of the adhesive layer, and eventually led to a reduction in the adhesive strength (Das and Pradhan 2011).

It should be noted that there were certain assumptions made during the analysis (Hao *et al.* 2018). For example, the WP/PE was assumed to be isotropic, but in the actual extrusion process, wood flour would have a certain directional alignment along the extrusion direction, which would make the whole composite anisotropic to a certain degree. Additionally, the adhesives were typical viscoelastic materials, which were assumed to be elastic materials in this study. These assumptions made the finite element simulation results deviate from a real situation, but because the peeling stress and shear stress of the bonded joints are difficult to measure through experiments, the finite element simulation of the joint stress can still be used as a reference for the design of bonded structures (Feng *et al.* 2014).

CONCLUSIONS

1. After the plasma surface treatment, polar oxygen-containing groups, such as -OH, C=O, and C=O, were introduced to the surface of the WP/PE, which improved the bonding effect of the WP/PE single lap adhesive joint and achieved effective connection of the WP/PE adhesive interface. The failure form of the adhesive joint was mainly a mixed failure mode, and the failure form of the end of the lap joint area was all material body failure.
2. The distributions of the Mises equivalent stress, peeling stress, and shear stress of the WP/PE single lap adhesive joint were mainly concentrated at the end of the adhesive joint, and the end of the lap zone was the fracture failure point of the adhesive joint.
3. The stress distribution of the WP/PE single lap adhesive joint mainly depended on the elastic modulus of the adhesive. Adhesives with different moduli had a great influence on the Mises equivalent stress, peeling stress, and shear stress distribution of the WP/PE single lap adhesive joint. The peak stress of the high-modulus epoxy resin adhesive joint was higher than that of the low-modulus acrylic ester adhesive. Also, the change in the length and size of the lap zone had a weak influence on the stress distribution.
4. In the finite element simulation, the applied load should be within the failure limit of the adhesive joint. The results of finite element simulation can quickly determine the stress concentration position of adhesive joint in service, which is an important supplement to the research of adhesive joint.
5. It was feasible to treat the WP/PE surface by plasma discharge in the bonding structure design of WP/PE. Acrylic ester adhesive with a low modulus of elasticity should be used in the bonding structure design of WP/PE when used in small size change positions, such as building or arc structures.

ACKNOWLEDGMENTS

This study was supported by the National Natural Science Foundation of China (Grant No. 31670567) and the Fundamental Research Funds for the Central Universities of China (2572017EB06).

REFERENCES CITED

- Ashori, A. (2008). "Wood-plastic composites as promising green-composites for automotive industries," *Bioresour. Technol.* 99(11), 4661-4667. DOI: 10.1016/j.biortech.2007.09.043
- ASTM D638-14 (2015). "Standard test method for tensile properties of plastics," ASTM International, West Conshohocken, PA.
- ASTM D905-08 (2013). "Standard test method for strength properties of adhesive bonds in shear by compression loading," ASTM International, West Conshohocken, PA.
- Ayatollahi, M. R., Samari, M., Razavi, S. M. J., and da Silva, L. F. M. (2017). "Fatigue performance of adhesively bonded single lap joints with non-flat sinusoid interfaces," *Fatigue Fract. Eng. M.* 40(9), 1355-1363. DOI: 10.1111/ffe.12575

- Cheng, R. X., Wang, Q. W., and Zhang, L. (2012a). "Bonding properties of poly (vinyl chloride)-based wood-plastic composites bonded with epoxy adhesives," *J. Appl. Polym. Sci.* 125(1), 175-179. DOI:10.1002/app.35385
- Cheng, R. X., Zhang, L., and Li, Y. (2012b). "Study on bonding properties of PVC-based WPC bonded with acrylic adhesive," *J. Adhes. Sci. Technol.* 26(24), 2729-2735. DOI:10.1080/01694243.2012.701477
- da Silva, L. F. M., Ferreira, N. M. A. J., Richter-Trummer, V., and Marqu, E. A. S. (2010). "Effect of grooves on the strength of adhesively bonded joints," *Int. J. Adhes. Adhes.* 30(8), 735-743. DOI: 10.1016/j.ijadhadh.2010.07.005
- Das, R. R., and Pradhan, B. (2011). "Finite element based design and adhesion failure analysis of bonded tubular socket joints made with laminated FRP composites," *J. Adhes. Sci. Technol.* 25(1-3), 41-67. DOI: 10.1163/016942410X508073
- Dimitriou, A., Hale, M. D., and Spear, M. J. (2016). "The effect of four methods of surface activation for improved adhesion of wood polymer composites (WPCs)," *Int. J. Adhes. Adhes.* 68, 188-194. DOI: 10.1016/j.ijadhadh.2016.03.003
- Feng, P., Zhang, P., Meng, X., and Ye, L. (2014). "Mechanical analysis of stress distribution in a carbon fiber-reinforced polymer rod bonding anchor," *Polymers* 6(4), 1129-1143. DOI: 10.3390/polym6041129
- Goglio, L., Rossetto, M., and Dragoni, E. (2008). "Design of adhesive joints based on peak elastic stresses," *Int. J. Adhes. Adhes.* 28(8), 427-435. DOI: 10.1016/j.ijadhadh.2008.04.001
- Gupta, B. S., and Laborie, M.-P. G. (2007). "Surface activation and adhesion properties of wood-fiber reinforced thermoplastic composites," *J. Adhesion.* 83(11), 939-955. DOI: 10.1080/00218460701751814
- Gupta, B. S., Reiniati, I., and Laborie, M.-P. G. (2007). "Surface properties and adhesion of wood fiber reinforced thermoplastic composites," *Colloid. Surface. A* 302(1-3), 388-395. DOI: 10.1016/j.colsurfa.2007.03.002
- Hao, X. L., Zhou, H. Y., Xie, Y. J., Mu, H. L., and Wang, Q. W. (2018). "Sandwich-structured wood flour/HDPE composite panels: Reinforcement using a linear low-density polyethylene core layer," *Constr. Build. Mater.* 164, (489-496). DOI: 10.1016/j.conbuildmat.2017.12.246
- Huang, R. Z., Xiong, W., Xu, X. W., and Wu, Q. L. (2012). "Thermal expansion behavior of co-extruded wood-plastic composites with glass-fiber reinforced shells," *BioResources* 7(4), 5514-5526. DOI: 10.15376/biores.7.4.5514-5526
- Hung, K.-C., Yeh, H., Yang, T.-C., Wu, T.-L., Xu, J.-W., and Wu, J.-H. (2017). "Characterization of wood-plastic composites made with different lignocellulosic materials that vary in their morphology, chemical composition and thermal stability," *Polymers.* 9(12), 726. DOI: 10.3390/polym9120726
- Hünnekens, B., Avramidis, G., Ohms, G., Krause, A., Viöl, W., and Militz, H. (2018). "Impact of plasma treatment under atmospheric pressure on surface chemistry and surface morphology of extruded and injection-molded wood-polymer composites (WPC)," *Appl. Surf. Sci.* 441, 564-574. DOI: 10.1016/j.apsusc.2018.01.294
- Li, Z. F. (2012). "Mechanical analysis of tubing string in well testing operation," *J. Petrol. Sci. Eng.* 90-91, 61-69. DOI: 10.1016/j.petrol.2012.04.019
- Liu, Y., Tao, Y., Lv, X., Zhang, Y., and Di, M. (2010). "Study on the surface properties of wood/polyethylene composites treated under plasma," *Appl. Surf. Sci.* 257(3), 1112-1118. DOI: 10.1016/j.apsusc.2010.08.032

- Mekaouche, A., Chapelle, F., and Balandraud, X. (2015). "FEM-based generation of stiffness maps," *IEEE T. Robot.* 31(1), 217-222. DOI: 10.1109/TRO.2015.2392351
- Moritzer, E., and Hopp, M. (2017). "Bonding of wood-plastic composites (WPC)-material and surface modification for special applications," *Weld. World.* 61(5), 1029-1038. DOI: 10.1007/s40194-017-0487-0
- Nemeş, O., and Lachaud, F. (2010). "Double-lap adhesive bonded-joints assemblies modeling," *Int. J. Adhes. Adhes.* 30(5), 288-297. DOI: 10.1016/j.ijadhadh.2010.02.006
- Noeske, M. P. L., Degenhardt, J., Sturdthoff, S., and Lommatzsch, U. (2004). "Plasma jet treatment of five polymers at atmospheric pressure: Surface modifications and the relevance for adhesion," *Int. J. Adhes. Adhes.* 24(2), 171-177. DOI: 10.1016/j.ijadhadh.2003.09.006
- Oporto, G. S., Gardner, D. J., Bernhardt, G., and Neivandt, D. J. (2007). "Characterizing the mechanism of improved adhesion of modified wood plastic composite (WPC) surfaces," *J. Adhes. Sci. Technol.* 21(11), 1097-1116. DOI: 10.1163/156856107782105954
- Ozdemir, T., and Mengeloglu, F. (2008). "Some properties of composites panels made from wood flour and recycled polyethylene," *Int. J. Mol. Sci.* 9(12), 2559-2569. DOI: 10.3390/ijms9122559
- Özer, H., and Öz, O. (2012). "Three dimensional finite element analysis of bi-adhesively bonded double lap joint," *Int. J. Adhes. Adhes.* 37, 50-55. DOI: 10.1016/j.ijadhadh.2012.01.016
- Panigrahi, S. K. (2013). "Structural design of single lap joints with delaminated FRP composite adherends," *Compos. Part B-Eng.* 51, 112-120. DOI: 10.1016/j.compositesb.2013.03.039
- Perišić, M., Radojević, V., Uskoković, P. S., Stojanović, D., Jokić, B., and Aleksić, R. (2009). "Wood-thermoplastic composites based on industrial waste and virgin high-density polyethylene (HDPE)," *Mater. Manuf. Process.* 24(10-11), 1207-1213. DOI: 10.1080/10426910903032212
- Ribeiro, T. E. A., Campilho, R. D. S. G., da Silva, L. F. M., and Goglio, L. (2016). "Damage analysis of composite-aluminium adhesively-bonded single-lap joints," *Compos. Struct.* 136, 25-33. DOI: 10.1016/j.compstruct.2015.09.054
- Santoni, A., Bonfiglio, P., Mollica, F., Fausti, P., Pompoli, F., and Mazzanti, V. (2018). "Vibro-acoustic optimisation of wood plastic composite systems," *Constr. Build. Mater.* 174, 730-740. DOI: 10.1016/j.conbuildmat.2018.04.155
- Sayman, O., Ozen, M., and Korkmaz, B. (2013). "Elasto-plastic stress distributions in adhesively bonded double lap joints," *Mater. Design* 45, 31-35. DOI: 10.1016/j.matdes.2012.9669.09.005
- Sen, F., and Köksal, H. (2015). "Three dimensional stress analysis of adhesively bonded and multi pinned metal matrix composite plates," *Mater. Test.* 57(6), 551-557. DOI: 10.3139/120.110746
- Shahin, K., and Taheri, F. (2009). "Deformations in adhesively bonded joints on elastic foundations," *Compos. Struct.* 90(2), 130-140. DOI: 10.1016/j.compstruct.2009.02.011
- Soroceanu, M., Barzic, A. I., Stoica, I., Sacarescu, L., Ioanid, E. G., and Harabagiu, V. (2017). "Plasma effect on polyhydrosilane/metal interfacial adhesion/cohesion interactions," *Int. J. Adhes. Adhes.* 74, 131-136. DOI: 10.1016/j.ijaahadh.2017.01.009

- Sülü, I. Y. (2018). “Mechanical behavior of composite parts adhesively jointed with the insert double-lap joint under tensile load,” *Weld. World*. 62(2), 403-413. DOI: 10.1007/s40194-017-0543-9
- Tang, H. Q., and Liu, L. Q. (2018). “A novel metal-composite joint and its structural performance,” *Compos. Struct.* 206, 33-41. DOI: 10.1016/j.compstruct.2018.07.111
- Vaidya, U. K., Serrano, J. C., Villalobos, A., Sands, J., and Garner, J. (2008). “Design and analysis of a long fiber thermoplastic composite tailcone for a tank gun training round,” *Mater. Design*. 29(2), 305-318. DOI: 10.1016/j.matdes.2007.02.010
- Wolkenhauer, A., Avramidis, G., Hauswald, E., Militz, H., and Viöl, W. (2008). “Plasma treatment of wood-plastic composites to enhance their adhesion properties,” *J. Adhes. Sci. Technol.* 22(16), 2025-2037. DOI: 10.1163/156856108X332543
- Wong, E.-H., and Liu, J. (2017). “Design analysis of adhesively bonded structures,” *Polymers* 9(12), 664. DOI: 10.3390/polym9120664
- Xará, J. T. S., and Campilho, R. D. S. G. (2018). “Strength estimation of hybrid single-L bonded joints by the extended finite element method,” *Compos. Struct.* 183, 397-406. DOI: 10.1016/j.compstruct.2017.04.009
- Yáñez-Pacios, A. J., and Martín-Martínez, J. M. (2018). “Comparative adhesion, ageing resistance, and surface properties of wood plastic composite treated with low pressure plasma and atmospheric pressure plasma jet,” *Polymers*. 10(6), 643. DOI: 10.3390/polym10060643
- You, M., Zheng, Y., Zheng, X.-L., and Liu, W.-J. (2003). “Effect of metal as part of fillet on the tensile shear strength of adhesively bonded single lap joints,” *Int. J. Adhes. Adhes.* 23(5), 365-369. DOI: 10.1016/S0143-7496(03)00064-2
- Zhang, Y., Zhang, K., Zhao, H., Xin, J., and Duan, M. (2018). “Stress analysis of adhesive in a cracked steel plate repaired with CFRP,” *J. Constr. Steel Res.* 145, 210-217. DOI: 10.1016/j.jcsr.2018.02.029

Article submitted: January 2, 2019; Peer review completed: May 13, 2019; Revised version received: May 20, 2019; Accepted; May 31, 2019; Published: June 10, 2019. DOI: 10.15376/biores.14.3.5908-5922